J. Fluid Mech. (1969), *vol.* 36, *part* 2, *pp.* 239–256
Printed in Great Britain

Buoyancy-driven convection in cylindrical geometries

By S. F. LIANG, A. VIDAL† AND ANDREAS ACRIVOS
Department of Chemical Engineering, Stanford University, California

(Received 23 January 1968 and in revised form 24 September 1968)

Numerical solutions to the Boussinesq equations containing a temperature-dependent viscosity are presented for the case of axisymmetric buoyancy-driven convective flow in a cylindrical cell. Two solutions, one with upflow and the other with downflow at the centre of the cell, were found for each set of boundary conditions that were considered. The existence of these two steady-state régimes was verified experimentally for the case of a cylindrical cell having rigid insulating lateral boundaries and isothermal top and bottom planes.

Using a perturbation expansion it is also shown that only one of these solutions remains stable in the subcritical régime. This, however, seems to be confined to a very narrow range of Rayleigh numbers, beyond which, according to all the evidence presently at hand, both solutions are equally stable for those values of the Rayleigh and Prandtl numbers for which axisymmetric motions occur.

Finally, certain fundamental differences between the problem considered here and that of thermal convection in a layer of infinite horizontal extent are briefly discussed.

1. Introduction

The occurrence of convective motions in horizontal layers of fluid heated from below has been a source of continual study for over half a century. Generally, one associates the names of Bénard and Rayleigh with this phenomenon. The former was the first to report on the highly regular structure assumed by the medium owing to thermal convection, whereas the latter, using a linearized stability analysis, was the first to predict theoretically certain key features of this convective flow for the case of fluid layers of infinite horizontal extent subject to buoyancy forces. Rayleigh's work has long served as the basis for more detailed linear treatments such as those put forth by Pellew & Southwell (1940), Sparrow, Goldstein & Jonsson (1964) and Hurle, Jakeman & Pike (1967); however, an explanation of some of the most remarkable aspects of these convective motions, for example the preferred shape and size of the cellular structure and the direction of circulation inside the cells, lies beyond the reach of linear stability theory.

Specifically, the present work is concerned with the generally accepted view regarding the effect that a temperature-dependent viscosity has upon the direction of the circulating fluid. Graham (1933) was the first to suggest that the direction of flow in cellular convection was determined by the variation of the

† Present address: Chicago Bridge and Iron, Plainfield, Illinois.

viscosity with temperature, and was such that the fluid motion at the centre of the cell was in the direction of increasing kinematic viscosity. This hypothesis seems to have been further strengthened by Tippelskirch's (1956) experiments using liquid sulphur (the viscosity of which increases sharply with temperature in the range 153–190 °C while decreasing with temperature everywhere else) in which flow reversal was noted when the temperature exceeded 153 °C. However, this matter was settled only recently for the case of thermal convection in a layer of infinite horizontal extent, thanks to the non-linear analyses of Palm (1960), Segel & Stuart (1962), Palm & Øiann (1964), Segel (1965), Busse (1967) and Palm, Ellingsen & Gjevik (1967).

In what follows, the question of whether, and if so to what extent, the temperature coefficient of the viscosity does in fact determine any observed preferred direction of flow in buoyancy-driven cellular convection will be investigated for the case of axisymmetric motions in a cylindrical geometry. To this end, steady-state numerical solutions to the non-linear equations of momentum, mass and energy, incorporating a temperature-dependent viscosity, will be presented for a large variety of boundary conditions, following which certain key predictions from the numerical results will be compared with appropriate experimental observations in a cylindrical cell heated from below and having insulating lateral boundaries. Finally, the numerical and experimental findings regarding the sense of circulation will be compared with the predictions of an analytical solution which applies within a small region near the critical point of linear stability.

2. Numerical analysis

The mathematical model is set up in terms of the Boussinesq equations with $\rho = \rho_0(1-\beta(T-T_0))$ in the gravitational term and with a temperature-dependent viscosity of the form

$$\frac{\mu}{\mu_1} = 1+\eta\frac{T-T_1}{T_0-T_1}.$$

The fluid is assumed to be confined within the cylindrical region $0 \leqslant r' \leqslant r_a d$, $0 \leqslant z' \leqslant d$, having its lateral boundary $r' = r_a d$ insulated and its horizontal bounding surfaces $z' = 0$, d maintained, respectively, at constant temperatures T_0 and T_1.† Only axisymmetric motions will be considered since these lend themselves to a relatively straightforward numerical computation. Hence, expressing the steady-state equations of motion and heat transport in this modified Boussinesq approximation in terms of the dimensionless stream function ψ, the vorticity ω and the temperature $\hat{\theta}$ defined by

$$(z,r) = \left(\frac{z'}{d},\frac{r'}{d}\right), \quad (u_r,u_z) = \left(\frac{u_r'}{U},\frac{u_z'}{U}\right), \quad U = \frac{\mu_1}{\rho_0 d},$$

† In a few cases, the more general temperature boundary condition $(\partial\hat{\theta}/\partial z)+N_g\hat{\theta} = -1$ was employed at $z = 1$. Here N_g denotes the vapour-phase Nusselt number, with $N_g = \infty$ or 0 corresponding, respectively, to an isothermal or a constant-flux surface.

$$p = \frac{p'}{\rho_0 U^2}, \quad \hat{\theta} = \frac{T - T_1}{T_0 - T_1} = \frac{\bar{T} + T' - T_1}{T_0 - T_1} = \frac{T'}{T_0 - T_1} + 1 - z,$$

$$u_r = \frac{1}{r}\frac{\partial \psi}{\partial z}, \quad u_z = -\frac{1}{r}\frac{\partial \psi}{\partial r}, \quad w = \frac{\partial u_r}{\partial z} - \frac{\partial u_z}{\partial r},$$

the following set is obtained:

$$\omega = \frac{1}{r}\frac{\partial^2 \psi}{\partial z^2} + \frac{1}{r}\frac{\partial^2 \psi}{\partial r^2} - \frac{1}{r^2}\frac{\partial \psi}{\partial r}, \tag{1}$$

$$\frac{\partial^2 \hat{\theta}}{\partial r^2} + \frac{\partial^2 \hat{\theta}}{\partial z^2} + \frac{1}{r}\left(1 - P\frac{\partial \psi}{\partial z}\right)\frac{\partial \hat{\theta}}{\partial r} + \frac{P}{r}\frac{\partial \psi}{\partial r}\frac{\partial \hat{\theta}}{\partial z} = 0, \tag{2}$$

$$\begin{aligned}\frac{1}{r}\frac{\partial \psi}{\partial z}\frac{\partial \omega}{\partial r} - \frac{\omega}{r^2}\frac{\partial \psi}{\partial z} - \frac{1}{r}\frac{\partial \psi}{\partial r}\frac{\partial \omega}{\partial z} = &-\frac{R}{P}\frac{\partial \hat{\theta}}{\partial r} + (1 + \eta\hat{\theta})\left(\frac{\partial^2 \omega}{\partial r^2} + \frac{1}{r}\frac{\partial \omega}{\partial r} - \frac{\omega}{r^2} + \frac{\partial^2 \omega}{\partial z^2}\right) \\ &+ 2\eta\left\{\frac{\partial \hat{\theta}}{\partial z}\frac{\partial \omega}{\partial z} + \frac{\partial \hat{\theta}}{\partial r}\left(\frac{\partial \omega}{\partial r} + \frac{\omega}{2r}\right) + \frac{\partial^2 \hat{\theta}}{\partial r\,\partial z}\left(\frac{2}{r}\frac{\partial^2 \psi}{\partial r\,\partial z} - \frac{1}{r^2}\frac{\partial \psi}{\partial z}\right)\right\} \\ &+ \eta\left(\frac{\partial^2 \hat{\theta}}{\partial z^2} - \frac{\partial^2 \hat{\theta}}{\partial r^2}\right)\left(\frac{2}{r}\frac{\partial^2 \psi}{\partial z^2} - \omega\right),\end{aligned} \tag{3}$$

where P and R are, respectively, the Prandtl and the Rayleigh numbers

$$P = \frac{\rho_0 c_p \mu_1}{k}, \quad R = \frac{g\beta(T_0 - T_1)d^3 \rho_0^2 c_p}{\mu_1 k},$$

g is the acceleration of gravity and k and c_p are the thermal conductivity and the heat capacity of the fluid assumed constant. These equations were next approximated by finite differences using the centred three-point expressions for both first and second derivatives and then rearranged into iteration formulas for the computation of successive values of the stream function, the temperature and the vorticity. Both the r- and the z-axes were subdivided into equal intervals. As for the boundary conditions, these were written using an uncentred derivative form so that the conditions on the boundaries of the computational region were expressed in terms of the adjacent points within the domain.

The numerical calculations were begun by setting the vorticity and the stream function equal to zero and by imposing an initial temperature profile of the form

$$\hat{\theta} = (1 - z)[1 + A(r - r^2)], \tag{4}$$

with $|A| \leqslant 1$ and $\hat{\theta}$ replaced by 1 whenever the right-hand side exceeded unity. The iterations were then continued by means of a straightforward relaxation technique until, after two successive iterations, the relative change of all the corresponding quantities within the domain became everywhere less than one part in a thousand.

The accuracy of the numerical solution was inferred by comparing the average Nusselt numbers $\bar{N}_0$ and $\bar{N}_1$, defined by

$$\bar{N}_{0,1} = \frac{2}{r_a^2}\int_0^{r_a} r \left|\frac{\partial \hat{\theta}}{\partial z}\right|_{z=0,1} dr,$$

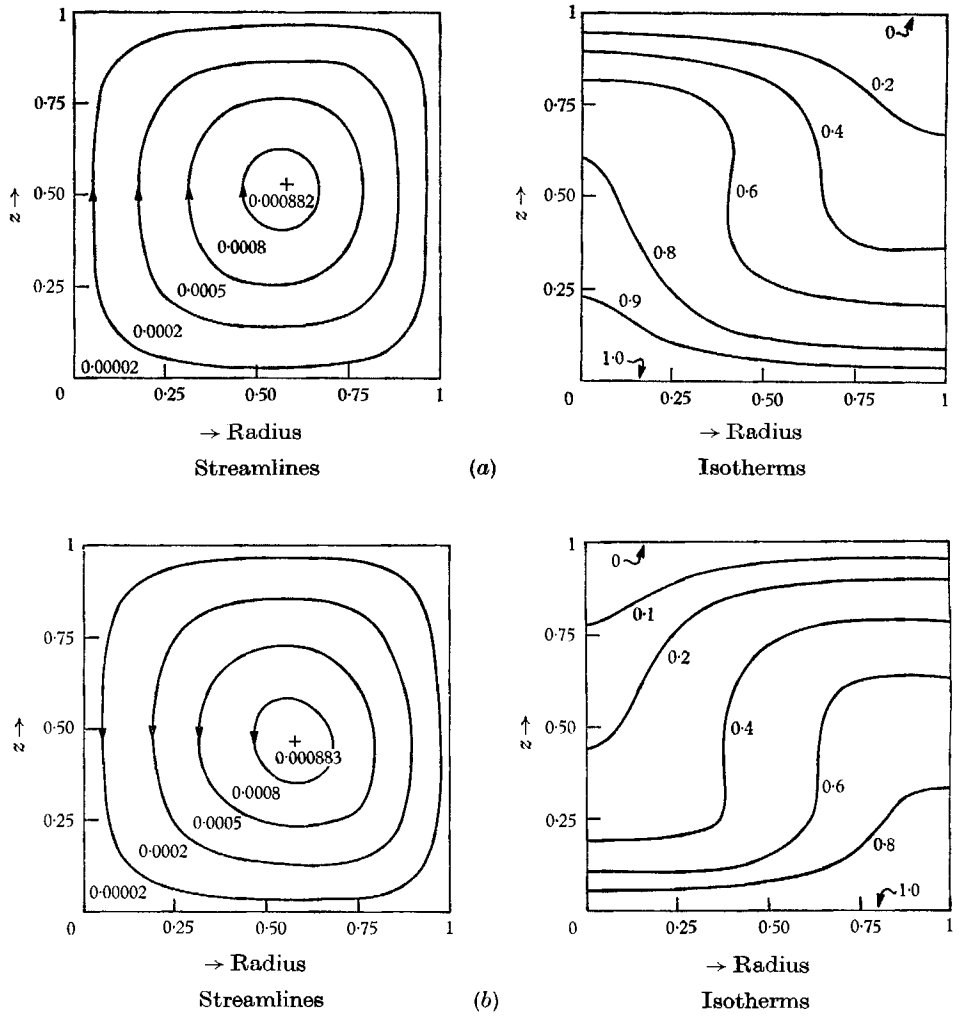

FIGURE 1. Streamlines and isotherms. (*a*) Upflow at the centre. Run no. 1 (table 1). (*b*) Downflow at the centre. Run no. 1 (table 1).

which, owing to energy conservation requirements, should be identical. This condition was met in all the cases to be reported below, where $\bar{N}_0$ and $\bar{N}_1$ were always within 1% of one another.

As seen in table 1, which summarizes all the cases treated numerically, calculations were performed for numerous combinations of P, R and η, and for both solid and free upper, lower and lateral boundaries. Here, the open entries represent cases for which numerical solutions were not obtained because it was felt that these would yield little if any new information regarding the nature of the steady flow, and also because of the excessive computational time necessary for convergence (this was particularly true for values of R close to the critical, as in run 16, where a large increase in the time required for convergence was noted as the critical point was approached). Also, for any given set of boundary conditions,

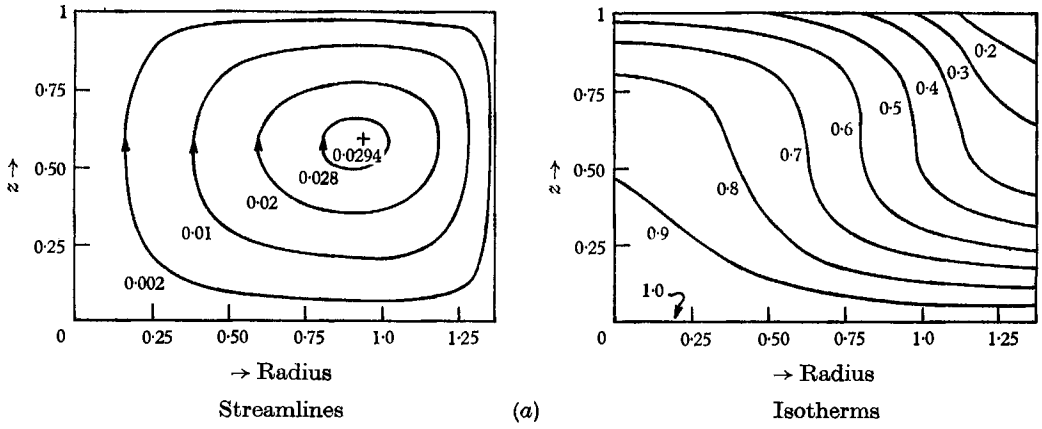

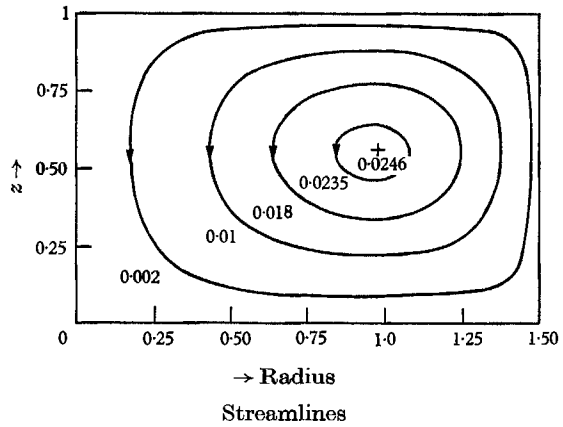

FIGURE 2. Streamlines and isotherms. (*a*) Upflow at the centre. Run no. 14 (table 1). (*b*) Downflow at the centre. Run no. 15 (table 1).

Run no.	Lateral surface $r = r_a$ insulated: Solid	Lateral surface $r = r_a$ insulated: Free	Lower surface isothermal: Solid	Lower surface isothermal: Free	Upper surface: Solid	Upper surface: Free	N_g	η	R	P	$\lvert\psi\rvert_{\max}$: Upflow at centre	$\lvert\psi\rvert_{\max}$: Downflow at centre	$\bar{N} = \frac{1}{2}(\bar{N}_0 + \bar{N}_1)$: Upflow at centre	$\bar{N} = \frac{1}{2}(\bar{N}_0 + \bar{N}_1)$: Downflow at centre	Mesh
1	×	—	×	—	×	—	∞	−0·2	5000	2500	0·000882	0·000883	1·767	1·761	19 × 19
2	×	—	×	—	×	—	0	−0·4	4000	250	0·00614	0·00593	1·010	1·008	19 × 19
3	—	×	×	—	×	—	∞	0	4000	100	0·0225	0·0225	1·836	1·836	29 × 29
4	—	×	×	—	×	—	∞	−0·2	4000	100	0·0250	0·0250	1·942	1·933	29 × 29
5	—	×	×	—	×	—	∞	−0·4	4000	100	0·0276	0·0281	2·038	2·049	29 × 29
6	—	×	×	—	×	—	∞	0·2	4000	100	0·0203	0·0203	1·741	1·750	29 × 29
7	—	×	×	—	×	—	∞	0·4	4000	100	0·0183	0·0185	1·653	1·675	29 × 29
8	—	×	×	—	×	—	∞	0·4	4000	10	—	0·1844	—	1·662	19 × 19
9	—	×	×	—	×	—	∞	0	4000	1	2·151	2·136	1·784	1·777	19 × 19
10	—	×	×	—	×	—	∞	−0·4	4000	1	2·598	2·739	1·983	1·998	19 × 19
11	—	×	×	—	×	—	∞	0·4	4000	1	1·766	1·763	1·618	1·624	19 × 19
12	—	×	×	—	×	—	∞	−0·4	2000	100	0·0118	0·0115	1·356	1·338	19 × 19
13	—	×	×	—	—	×	∞	0	4000	100	0·0310	0·0322	2·353	2·414	29 × 29
14	—	×	×	—	—	×	1	−0·3	1806	100	0·0292	—	1·314	—	22 × 16
15	—	×	×	—	—	×	0	−0·3	1567	100	0·0262	0·0247	1·010	1·009	24 × 16
16	—	×	—	×	—	×	∞	−0·2	700	10	0·1967	—	1·267	—	26 × 15

TABLE 1. Summary of numerical results

the parameter r_a was kept fixed at a value approximately equal to that given by the linear theory for the size of the cell at the critical point. A few representative streamlines and isotherms are shown in figures 1 and 2.

For the purpose of the present discussion, perhaps the most important result of these numerical computations was that, in every case considered, the iteration scheme was found to converge to either of two different steady-state solutions depending on the nature of the imposed initial temperature field. Thus, if the initial parabolic temperature disturbance was such as to increase the buoyancy near the centre of the cylindrical region, i.e. $A > 0$ in (4), the system converged to an axisymmetric solution in which the vertical velocity component was positive near the centre ($r = 0$) and negative near the lateral boundary ($r = r_a$). Conversely, if $A < 0$, the steady flow was downward near the centre and upward near the sides. These solutions have the following interesting properties:

(*a*) *Constant-viscosity case* ($\eta = 0$)

Let the subscripts d and u denote, respectively, the solutions with downflow or upflow at the centre. Then, provided the boundary conditions at $z = 0$ are identical with those at $z = 1$, direct substitution into (1) to (3) with $\eta = 0$ leads immediately to the result that

$$\{\psi_d(r,z), \theta'_d(r,z), \omega_d(r,z)\} = -\{\psi_u(r,1-z), \theta'_u(r,1-z), \omega_u(r,1-z)\}, \tag{5}$$

in which

$$\theta'(r,z) = \hat{\theta}(r,z) - (1-z).$$

In fact, again for symmetric boundary conditions, a similar transformation can be employed for any assumed flow pattern (e.g. hexagons in a fluid layer of infinite horizontal extent), thus establishing that, if one solution exists, a second solution must also be present having an opposite flow direction at the cell centres.

As expected, the numerical results were found to satisfy (5). However, for $P = 1$, the corresponding values agreed only to within 0·5 % because, owing to the higher velocities present, the time required for convergence of the numerical scheme increased to a point where it became impracticable to compute a completely convergent solution.

On the other hand, for the more general case of asymmetric boundary conditions, the presence of two solutions cannot be established analytically since (5) no longer applies. However, the fact that two apparently equally stable solutions were obtained numerically by an iterative technique which seemed to converge with equal ease to either one, does suggest strongly that two axisymmetric solutions do indeed exist in every case, irrespective of the boundary conditions at $z = 0$ and $z = 1$.

(*b*) *Variable viscosity* ($\eta \neq 0$)

Once again (5) ceases to apply if $\eta \neq 0$ and, hence, it should be expected that the numerical solutions for upflow and downflow at the centre would be somewhat different if compared according to (5). This was confirmed by a detailed examination of the raw numerical data, which, for $|\eta| = 0{\cdot}4$, revealed differences as large as 30 % between like quantities. Surprisingly, though, some of the gross properties of the two solutions, such as the corresponding values for $\bar{N}$ and $|\psi|_{\max}$,

were always found to be approximately the same, as can be seen from table 1 and figures 1 and 2. The only exception appeared to be the location of the vortex centre, which, even for $\eta = 0$ but for symmetric boundary conditions, was found to be near the lateral boundary, somewhat above the centreline $z = \frac{1}{2}$ for the case of upflow at the centre and somewhat below for downflow. This asymmetry is evident in figure 1 and will be further examined in the next section dealing with the experimental work.

In conclusion, the most important result of the numerical calculations was the observation that the presence of a temperature-dependent viscosity in no way affected the stability or the rate of convergence of the numerical iteration, for either the upflow or the downflow case and for all the various combinations of boundary conditions investigated, thus strongly suggesting that two physically realizable solutions do in fact exist within that range of Rayleigh and Prandtl numbers for which axisymmetric motions in a cylindrical cell are permissible. This assertion was tested experimentally in the manner described below.

3. Experimental study

Experimental apparatus

The experiments were conducted in a cylindrical cell whose lateral wall consisted of a 0·64 cm thick lucite (methyl methacrylate) circular cylinder, 3 cm high and 5·7 cm in internal diameter. One end of this cylinder was cemented to a 0·95 cm thick circular copper plate, of the same outside diameter as the lucite and containing two interior concentric channels through which water could be circulated. A similar copper plate with only one circular channel was used in some of the experiments to simulate a rigid isothermal top. Copper–constantan thermocouples embedded in the centre of the plates served to monitor their temperature. The working fluid was a very viscous oil—white oil 15, which has a temperature-dependent viscosity corresponding to $\eta \cong -0{\cdot}06$. Also, to simulate the numerical model (runs 1, 2), most of the experiments were restricted to flows consisting of a single convective cell and to overall vertical temperature differences of about 1 °C which gave values for R close enough to the critical Rayleigh number to ensure a steady motion.

Experimental procedure and results

(*a*) *Solid-isothermal upper surface.* The cylindrical cell was first filled with oil, at room temperature, containing small amounts of nitrogen-filled glass spheres, 13–15 μm in diameter, to serve as tracers. The cell was then covered with the copper plate and the whole system allowed to reach equilibrium. After this, the temperature difference between the top and bottom surfaces was gradually increased at a rate of less than 1 °C per hour, a time scale comparable to the characteristic time for unsteady heat conduction, by circulating cooling and heating water from two constant-temperature baths through the copper plates. Such a rate of heating was believed to be slow enough to allow the establishment of an approximately linear temperature profile prior to the onset of convection.

When the temperature difference between the top and the bottom plates reached, approximately, 0·5 °C, the fluid was seen to move, especially near the centre of the cell. In fact, the lowest temperature difference at which this motion could be detected was 0·45 °C, corresponding to a Rayleigh number of about 4300, which represents, therefore, an approximate upper bound for the stability criterion appropriate to this particular geometry. In addition, long time-exposures taken across different diameters of the cylinder for a wide range of values of the Rayleigh numbers (4300 to 12,000) showed that the particle paths were closed and axisymmetric, indicating that the overall flow pattern constituted a symmetric toroidal cell. Occasionally, and only when large initial heating rates were used, two other flow patterns were seen which were asymmetric and which seemed to correspond to those observed earlier by Mitchell & Quinn (1966) in their experiments with gases in cylindrical geometries but at much higher Rayleigh numbers. However, these asymmetric motions, which were not steady in time and which tended to evolve slowly into a more or less symmetric toroidal flow, were never encountered at the lower heating rates (less than 1 °C per hour) used in most of the experiments.

It was found throughout the experiments that two axisymmetric flow patterns having opposite flow directions near the centreline could always be produced for the case of two isothermal horizontal surfaces. Moreover, it was observed that the sense of circulation appeared to depend only on the curvature of the isotherms of the conduction profile, in that, when the isotherms were convex from above, i.e. when the warmer fluid was near the centre, the resulting motion was one of upflow at the centre, with the reverse being true when the conduction isotherms were concave from above.

The fact that the lucite walls were somewhat imperfect insulators provided a means of establishing at will the curvature of the conduction isotherms. For example, by keeping the top and bottom plates slightly above room temperature, a lateral flux of heat away from the cylinder was set up at the vertical boundary which cooled the oil near the wall and thereby caused a small convexity to develop in the conductive temperature profile. Similarly, a small concavity in the isotherms could be brought about by cooling both the top and the bottom plates to a temperature slightly below that of the room. In order to keep these lateral heat fluxes small, one of the plates was always kept as close to room temperature as possible, thus ensuring that the temperature of the oil was never more than, approximately, 1 °C above or below that of the surrounding air.

Experiments were also performed to test the influence of this lateral wall flux on the stability of the axisymmetric motion. Thus, after a steady flow pattern was established, the direction of the heat flux at the vertical walls was reversed by slowly raising (or lowering) both the top and bottom copper plate temperatures at the same rate, until the mean temperature of the oil was slightly above (or below) that of the room. It was found that over a period of 3–4 h, by which time most of the tracers had either settled or become attached to the walls of the cylinder, both axisymmetric flow patterns remained unchanged by such disturbances.

Aside from the sense of circulation, another characteristic feature of the flow

pattern was the location of the vortex centre, which was always found to lie near the vertical walls and placed asymmetrically with respect to a horizontal plane passing through the centre of the cylinder. As can be seen from figure 3, plate 1, the vortex centre was located above the middle plane when the flow was upwards at the centre and below that plane when the flow was in the opposite direction, in qualitative agreement with the numerical results shown in figure 1. Moreover, the location of the vortex centre seemed to be independent of the Rayleigh number in the range 4300 to 12,000.

(*b*) *Free upper surface.* In this case, the experiments did not correspond exactly to the numerical computations because of our inability to effectively control the temperature of the free surface. Consequently, although the experimental procedure was almost identical with that described above, the temperature of the lower copper plate had to be increased slowly but continuously in order to maintain a given Rayleigh number. Thus truly steady-state experiments could not be performed.

Motion was detected for values of R as low as about 3200, which, for these particular boundary conditions, can be taken as an approximate upper bound for the critical Rayleigh number. In addition, for extremely high rates of heating (more than 5 °C/h) an asymmetric flow pattern resembling a slightly deformed longitudinal roll was sometimes observed at the maximum depth (3 cm) but never for smaller depths or slower rates of heating.

The only flow pattern that was encountered regardless of depth for rates of heating of approximately 1 °C/h was an axisymmetric toroidal cell very similar to that observed in the case of two solid isothermal bounding surfaces. Moreover, for mean oil temperatures higher than that of the surroundings, the motion was always upwards near the centre of the cell, a fact which is consistent with the presence of convex pre-convective temperature profiles. This flow pattern was stable regardless of the magnitude of the Rayleigh number and was observed for hours without any sign of decay or transformation into an asymmetric motion.

Methods were also found for producing concave conduction profiles and thereby generating a flow pattern descending along the centre. One such technique consisted of using fairly large heating rates (around 4 °C per hour) and taking advantage of the fact that lucite has a thermal diffusivity approximately 15 % larger than that of the oil. Thus, depending on the magnitude of the heating rate, the lucite wall could be made warmer than the oil at the onset of convection, thereby setting up an axisymmetric flow pattern with the fluid moving downwards near the centre of the cell. This type of motion, once established, persisted for more than 1 h. Eventually, however, it was replaced by a transitory state having the appearance of a random flow of small amplitude, which later evolved into a symmetric motion with liquid moving upwards at the centre of the cell. Nevertheless, it is felt that, if the heat flux at the lateral wall could have been eliminated, this axisymmetric flow pattern with downflow at the centre could also have been maintained for indefinite periods of time.

4. Non-linear analysis

The numerical and experimental work described so far seems to have established rather conclusively that, in a cylindrical cell containing a fluid subject to buoyancy forces, two stable axisymmetric flow patterns are possible for values of the Rayleigh number exceeding the critical. This result may, however, not be applicable when the Rayleigh number is only slightly above the critical since, for obvious reasons, neither the experiments nor the numerical calculations could be extended right up to the critical point. It was felt, therefore, that a closer investigation of the present problem in the Rayleigh number régime near the critical point would be desirable, since such a study would serve to complement the numerical and experimental work already described. This was accomplished, using the perturbation technique developed by Busse (1967), for the mathematically simplest case of a free and insulating lateral boundary at $r = r_a$, and free and isothermal horizontal bounding surfaces at $z = 0$ and $z = 1$.

The analysis is of course complicated by the fact that, besides developing an analytic solution to the steady-state non-linear equations governing the convective motion, it is necessary that the stability of this flow to small disturbances be also examined. However, following Busse, it is possible to achieve both these objectives for small values of $R - R_c$ ($R_c = \frac{27}{4}\pi^4(1 + \frac{1}{2}\eta + O(\eta^2))$ denoting the critical Rayleigh number according to linear theory), by means of the formal series expansions in terms of ϵ, the amplitude of the steady motion, and η,

$$\left.\begin{aligned} R &= \sum_{\nu=0}^{\infty}\sum_{\mu=0}^{\infty} \epsilon^{\nu}\eta^{\mu} R_{\nu\mu}, \\ \hat{\theta} &= 1 - z + \sum_{\nu=1}^{\infty}\sum_{\mu=0}^{\infty} \epsilon^{\nu}\eta^{\mu}\theta_{\nu\mu}, \\ \psi &= \frac{1}{P}\sum_{\nu=1}^{\infty}\sum_{\mu=0}^{\infty} \epsilon^{\nu}\eta^{\mu}\psi_{\nu\mu}, \end{aligned}\right\} \tag{6}$$

for the primary flow, and

$$\left.\begin{aligned} \hat{\theta}' &= e^{\sigma t}\sum_{\nu=1}^{\infty}\sum_{\mu=0}^{\infty} \epsilon^{\nu}\eta^{\mu}\tilde{\theta}_{\nu\mu}, \\ \psi' &= \frac{1}{P}e^{\sigma t}\sum_{\nu=1}^{\infty}\sum_{\mu=0}^{\infty} \epsilon^{\nu}\eta^{\mu}\tilde{\psi}_{\nu\mu}, \end{aligned}\right\} \tag{7}$$

with

$$\sigma = \sum_{\nu=0}^{\infty}\sum_{\mu=0}^{\infty} \epsilon^{\nu}\eta^{\mu}\sigma_{\nu\mu}$$

for the disturbance. These series, when substituted into the system of non-linear equations, yield a set of inhomogeneous equations to which, in general, a solution does not exist unless the quantities $R_{\nu\mu}$ are chosen so as to satisfy an appropriate solvability condition. The coefficients $\sigma_{\nu\mu}$, which determine the stability of the primary flow, can then be obtained in a straightforward manner.

To conform with the numerical and experimental work, r_a was kept fixed at 1·725, the value given by the linear constant property solution for the size of the cell at the critical point (Pellew & Southwell 1940). Also, the analysis dealt only with axisymmetric motions since it is known that asymmetric flows are strongly

damped near the critical point. And, finally, only axisymmetric disturbances were taken into account, because, for a region enclosed by a cylindrical boundary of fixed size, these are the only disturbances, satisfying the boundary conditions and the equations of motion and energy, that can possibly arise. For example, since only axisymmetric small disturbances ψ_{10} and θ_{10} need to be considered near the critical point, in view of the fact that the corresponding asymmetric disturbances are strongly damped, it can easily be shown that ψ_{11} and θ_{11} satisfy an equation of the form

$$\mathscr{L}(\psi_{11}, \theta_{11}) = H,$$

where $\mathscr{L}$ is a linear operator and H, which depends explicitly on ψ_{10} and θ_{10}, is independent of the polar angle ϕ. Hence, ψ_{11} and θ_{11}, and, by a similar argument, all succeeding terms in (7), must remain axisymmetric provided R is close enough to R_c.

As a result of many lengthy mathematical manipulations, the details of which can be obtained from the authors on request, it was found that:

$$\begin{aligned}
\psi_{10}(r,z) &= rJ_1[(\pi/\sqrt{2})r]\sin\pi z, & \tilde{\psi}_{10} &= \tilde{c}\psi_{10}(r,z),\\
\theta_{10}(r,z) &= -(\sqrt{2}/3\pi)J_0[(\pi/\sqrt{2})r]\sin\pi z, & \tilde{\theta}_{10} &= \tilde{c}\theta_{10}(r,z),\\
\psi_{20}(r,z) &= -\psi_{20}(r)\sin 2\pi z, & \tilde{\psi}_{20} &= 2\tilde{c}\psi_{20}(r,z),\\
\theta_{20}(r,z) &= -\theta_{20}(r)\sin 2\pi z, & \tilde{\theta}_{20} &= 2\tilde{c}\theta_{20}(r,z),\\
\psi_{11}(r,z) &= rJ_1[(\pi/\sqrt{2})r]\Phi(z), & \tilde{\psi}_{11} &= \tilde{c}\psi_{11}(r,z),\\
\theta_{11}(r,z) &= J_0[(\pi/\sqrt{2})r]\theta_{11}(z), & \tilde{\theta}_{11} &= \tilde{c}\theta_{11}(r,z),
\end{aligned}$$

where $\tilde{c}$ is an arbitrary constant, and $\psi_{20}(r)$, $\theta_{20}(r)$ and $\Phi(z)$, $\theta_{11}(z)$ are shown, respectively, in figures 4 and 5. Also, from the solvability conditions,

$$\left.\begin{aligned}
&R_{00} = \frac{27\pi^4}{4}, \quad R_{01} = \tfrac{1}{2}R_{00}, \quad R_{10} = 0,\\
&\sigma_{00} = \sigma_{01} = \sigma_{10} = 0,\\
&\sigma_{11} = -R_{11}\frac{2}{9\pi^2}\frac{P}{1+P}, \quad \sigma_{20} = -R_{20}\frac{4}{9\pi^2}\frac{P}{1+P},
\end{aligned}\right\} \tag{8}$$

with R_{11} and R_{20} seen plotted in figure 6.

The principal result of this analysis is then that

$$R - R_c = \epsilon\eta R_{11} + \epsilon^2 R_{20} + \ldots, \tag{9a}$$

$$\sigma = \epsilon\eta\sigma_{11} + \epsilon^2\sigma_{20} + \ldots, \tag{9b}$$

from which the amplitude of the stable motions can be computed as a function of R. For example, if in (9*a*) the third- and higher-order terms are neglected, then

$$\epsilon = -\frac{1}{2}\frac{R_{11}}{R_{20}}\eta \pm \sqrt{\left[\left(\frac{R_{11}\eta}{2R_{20}}\right)^2 + \frac{R-R_c}{R_{20}}\right]}. \tag{10}$$

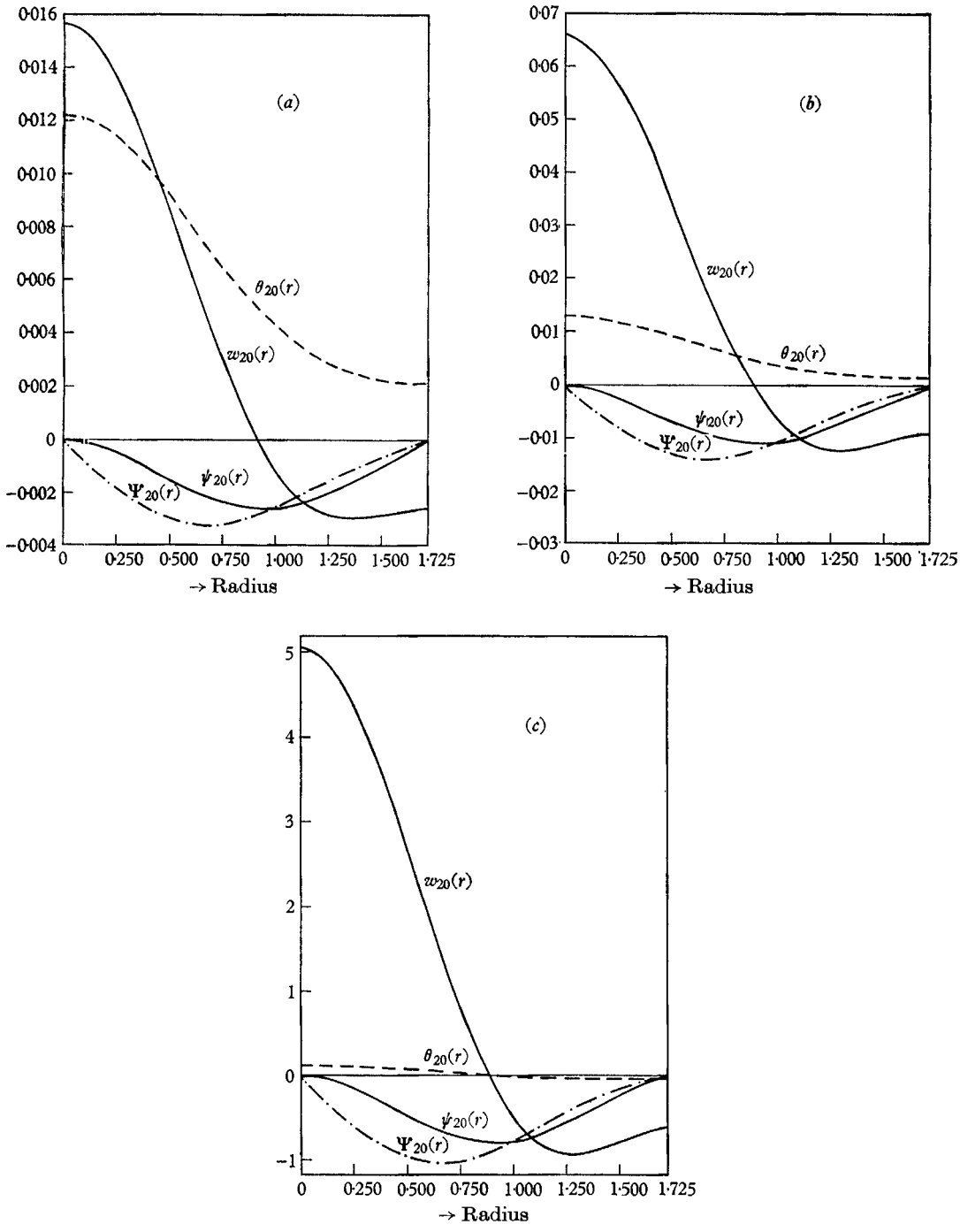

FIGURE 4. Order $(\epsilon^2\eta^0)$ solutions *vs.* Prandtl number.

$$\psi_{20} = -\psi_{20}(r) \sin 2\pi z, \qquad \theta_{20} = -\theta_{20}(r) \sin 2\pi z,$$

$$u_{20} = -2\pi\Psi_{20}(r) \cos 2\pi z, \quad w_{20} = -w_{20}(r) \sin 2\pi z.$$

(*a*) $P = 1000$. (*b*) $P = 1$. (*c*) $P = 0{\cdot}01$.

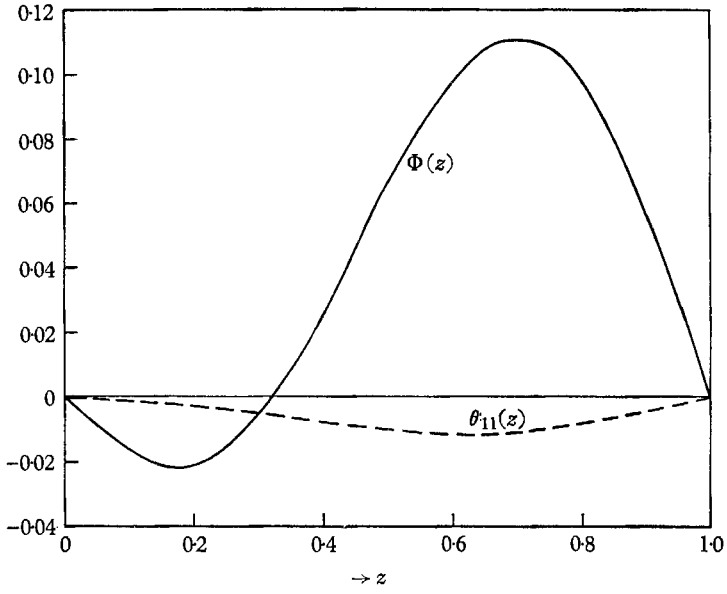

FIGURE 5. Order $(\epsilon^1\eta^1)$ solutions

$$\psi_{11} = rJ_1\left(\frac{\pi}{\sqrt{2}}r\right)\Phi(z), \quad \theta_{11} = J_0\left(\frac{\pi}{\sqrt{2}}r\right)\theta_{11}(z),$$

$$u_{11} = J_1\left(\frac{\pi}{\sqrt{2}}r\right)\Phi'(z), \quad w_{11} = -\frac{\pi}{\sqrt{2}}J_0\left(\frac{\pi}{\sqrt{2}}r\right)\Phi(z).$$

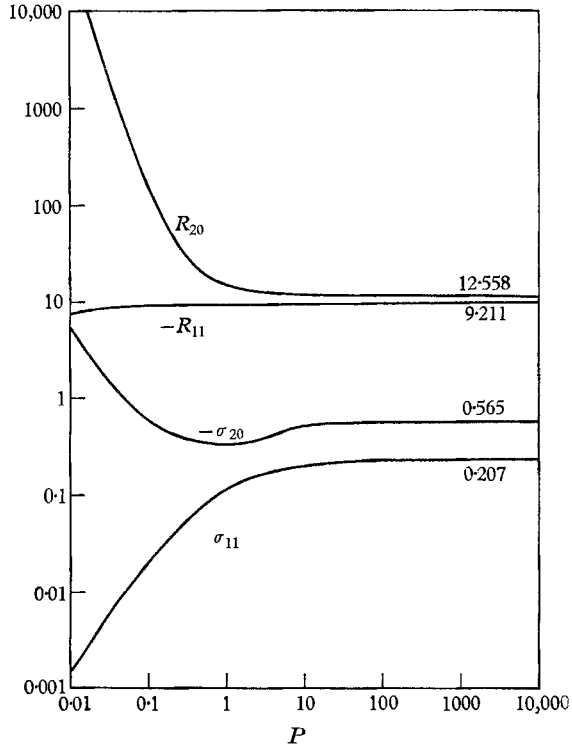

FIGURE 6. R_{20}, R_{11}, σ_{20}, σ_{11} *vs.* Prandtl number.

Two distinct cases arise depending on the sign of η.

(a) $\eta < 0$ (liquid case): equation (10) is seen plotted in figure 7(a). Clearly, since according to (8)

$$\left|\frac{\sigma_{11}}{\sigma_{20}}\right| = \frac{1}{2}\left|\frac{R_{11}}{R_{20}}\right|$$

for all Prandtl numbers, there exists one stable solution with upflow at the centre when R is in the range

$$-\left(\frac{R_{11}\eta}{2R_{20}}\right)^2 < \frac{R-R_c}{R_{20}} < 0$$

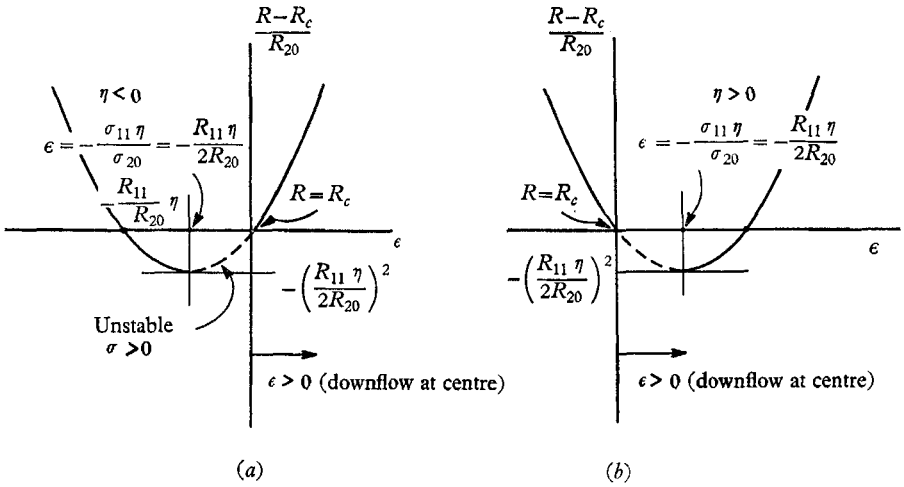

(a) (b)

FIGURE 7. $R-R_c$ *vs.* amplitude. (a) $\eta < 0$. (b) $\eta > 0$.

and two stable solutions, one with a higher amplitude and with upflow at the centre, the other with a smaller amplitude and with downflow at the centre, when the Rayleigh number is greater than R_c.

(b) $\eta > 0$ (gas case): equation (10), with $\eta > 0$, is seen plotted in figure 7(b). It is apparent that this case is identical to that considered above except that now the flow directions are reversed.

As concerns the rate of heat transport, this can best be expressed in terms of the Nusselt number N, where

$$N-1 = -\frac{2}{r_a^2}\int_0^{r_a}\left(\frac{\partial\theta}{\partial z}\right)_{z=0,1} r\,dr = \frac{4\pi}{r_a^2}\epsilon^2\int_0^{r_a}\theta_{20}(r)\,r\,dr$$

$$= \frac{4\pi}{r_a^2}\epsilon^2(6{\cdot}5\times 10^{-3}). \tag{11}$$

This expression is seen plotted in figure 8. Interestingly enough, although, in principle, (9) and (11) only apply if $\epsilon \ll 1$, the value for N as computed from (11) for $R = 700$, $\epsilon \sim 3$, is equal to 1·25, in very close agreement with the value 1·267 obtained from the numerical solution of the full equations (cf. table 1). This, however, is probably little more than a coincidence.

After the completion of the present analysis, it was called to the authors' attention that Müller (1965) had developed an approximate solution to the same problem using Galerkin's method and had arrived at the following results:

$$A_{11} = \frac{1}{2}\frac{\beta}{\alpha} \pm \sqrt{\left(\frac{\gamma + \frac{1}{4}\beta^2/\alpha}{\alpha}\right)},$$

with $\beta = 4{\cdot}47\eta$ and $\alpha = 2{\cdot}515$ for the case of infinite Prandtl number. In the notation of the present paper,

$$A_{11} = -\frac{\pi}{\sqrt{2}}\epsilon, \quad R_{20} = \frac{\pi^2}{2}\alpha, \quad R_{11} = -\frac{1}{\eta}\frac{\pi}{\sqrt{2}}\beta,$$

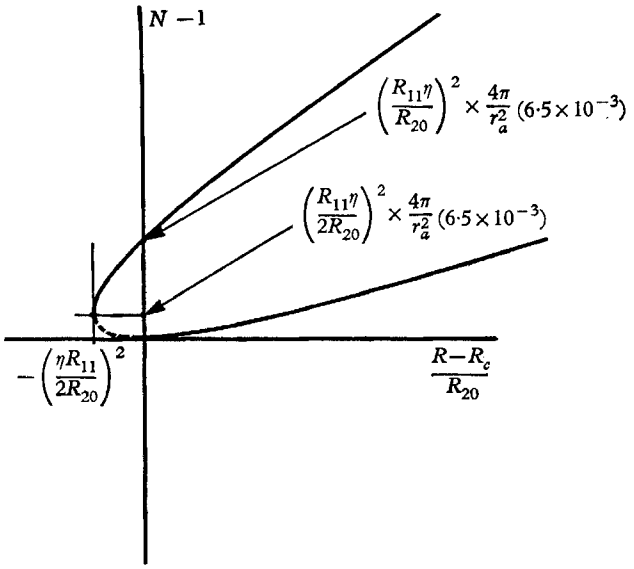

FIGURE 8. Nusselt number *vs.* the Rayleigh number near the critical point.

so that, according to Müller's solution, $R_{20} = 12{\cdot}4$ and $R_{11} = -9{\cdot}92$. These values compare very favourably with the more accurate results of the present study, according to which, for $P \gg 1$, $R_{20} = 12{\cdot}56$ and $R_{11} = -9{\cdot}22$.

The results obtained above are, in some sense, also qualitatively similar to those arrived at previously by Palm (1960), Segel & Stuart (1962), Palm & Øiann (1964), Segel (1965), Busse (1967) and Palm, Ellingsen & Gjevik (1967), for the problem of thermal convection with hexagonal cells in a fluid layer of infinite horizontal extent, in that, in both cases, only one of the two solutions is found to remain stable in the subcritical régime. However, the two cases do differ in one important respect in that the appropriate hexagonal solution remains unstable even beyond the critical point whereas, as seen in figure 7 (*a*) and (*b*), both solutions are stable in the present problem when $R > R_c$.

This disparity can easily be explained by referring to Busse (1967), who

showed that 'hexagonal' disturbances on a hexagonal cell of fixed size have growth constants given, respectively, by (in the present notation):

$$\left.\begin{aligned} \sigma_1 M &= -\epsilon\eta R_{11} - 2\epsilon^2 R_{20}, \\ \sigma_2 M &= \sigma_3 M = 2\epsilon\eta R_{11} + \tfrac{2}{3}\epsilon^2 L_2, \\ \sigma_4 M &= 3\epsilon\eta R_{11}, \\ \sigma_5 &= \sigma_6 = 0, \end{aligned}\right\} \tag{12}$$

where M and L_2 are positive constants. Clearly, the first of (12), which refers to the growth rate of an 'amplitude'-type disturbance, is identical with (9*b*) if account is taken of (8); in contrast, σ_2, σ_3 and σ_4 (which, incidentally, are responsible for the instability of the second solution even when $R > R_c$) have no counterpart in our analysis since here, as explained earlier, asymmetric disturbances are automatically excluded by the presence of a fixed cylindrical boundary. Thus it is perhaps not surprising that the hexagonal solution possesses a lower degree of stability than the cylindrical solution obtained here, since a layer of infinite horizontal extent is naturally subject to a much wider class of disturbances than the cylindrical layer considered here.

5. Conclusions

Steady-state numerical solutions to the non-linear equations of momentum, mass and energy, incorporating a temperature-dependent viscosity, were obtained for the case of buoyancy-driven convection in a cylindrical geometry and for various combinations of boundary conditions. Two axisymmetric solutions were found for each case considered. These two solutions, although exhibiting opposite flow directions at the centre of the cell, were similar in almost every other respect, thereby strongly suggesting that, for any given set of boundary conditions, two physically realizable solutions do in fact exist within the range of Rayleigh numbers investigated. This assertion was further strengthened by the experimental observation of two stable axisymmetric motions in a completely confined cylindrical cell.

An analytical solution using the perturbation technique described by Busse (1967) was also developed for Rayleigh numbers close to the critical. It was found that, for a fluid having a variable viscosity, subcritical flows exist for which only one of the steady-state solutions remains stable, but, since the range of Rayleigh numbers where this occurs is so narrow, i.e. $R - R_c \sim O(10)$, the existence of this region is probably of little more than academic interest. In fact, attempts to reach this region either experimentally or by means of a numerical solution of the basic equations proved quite unsuccessful, the latter because of the very rapid increase in the time required for convergence of the iteration scheme as the critical Rayleigh number was approached.

This work was supported in part by a grant from the Office of Saline Water. The authors are indebted to A. L. Hammond who initiated the numerical work and to F. Busse, A. E. Gill and E. Palm for their constructive criticisms of the first version of this paper.

REFERENCES

BUSSE, F. 1967 The stability of finite amplitude cellular convection and its relation to an extremum principle. *J. Fluid Mech.* **30**, 625–49.

GRAHAM, A. 1933 Shear patterns in an unstable layer of air. *Phil. Trans.* A **232**, 285–96.

HURLE, D. T. J., JAKEMAN, E. & PIKE, E. R. 1967 On the solution of the Bénard problem with boundaries of finite conductivity. *Proc. Roy. Soc.* A **296**, 469–75.

MITCHELL, W. T. & QUINN, J. A. 1966 Thermal convection in a completely confined fluid layer. *A.I.Ch.E. J.* **12**, 1116–24.

MÜLLER, U. 1965 Untersuchungen an rotationssymmetrischen Zellularkonvektionsströmungen II. *Beitr. Phys. Atm.* **38**, 9–22.

PALM, E. 1960 On the tendency towards hexagonal cells in steady convection. *J. Fluid Mech.* **8**, 183–92.

PALM, E., ELLINGSEN, T. & GJEVIK, B. 1967 On the occurrence of cellular motion in Bénard convection. *J. Fluid Mech.* **30**, 651–661.

PALM, E. & ØIANN, H. 1964 Contribution to the theory of cellular thermal convection. *J. Fluid Mech.* **19**, 353–65.

PELLEW, A. & SOUTHWELL, R. V. 1940 On maintained convective motion in a fluid heated from below. *Proc. Roy. Soc.* A **176**, 312–43.

SEGEL, L. A. 1965 The non-linear interaction of a finite number of disturbances to a layer of fluid heated from below. *J. Fluid Mech.* **21**, 359–84.

SEGEL, L. A. & STUART, J. T. 1962 On the question of the preferred mode in cellular thermal convection. *J. Fluid Mech.* **13**, 289–306.

SPARROW, E. M., GOLDSTEIN, R. J. & JONSSON, V. K. 1964 Thermal instability in a horizontal fluid layer: effect of boundary conditions and non-linear temperature profile. *J. Fluid Mech.* **18**, 513–28.

TIPPELSKIRCH, H. VON 1956 Über Konvektionszellen, insbesondere im flüssigen Schwefel. *Beitr. Phys. Atm.* **29**, 37–54.

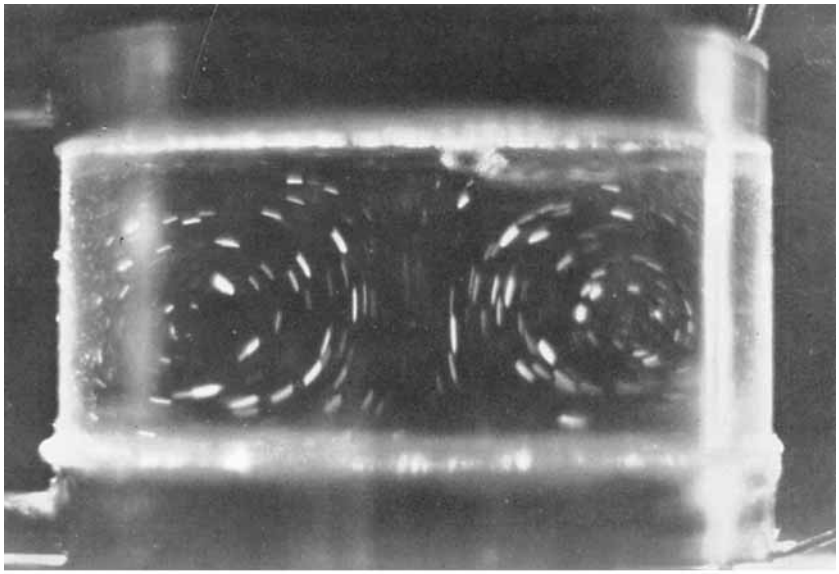

(*a*)

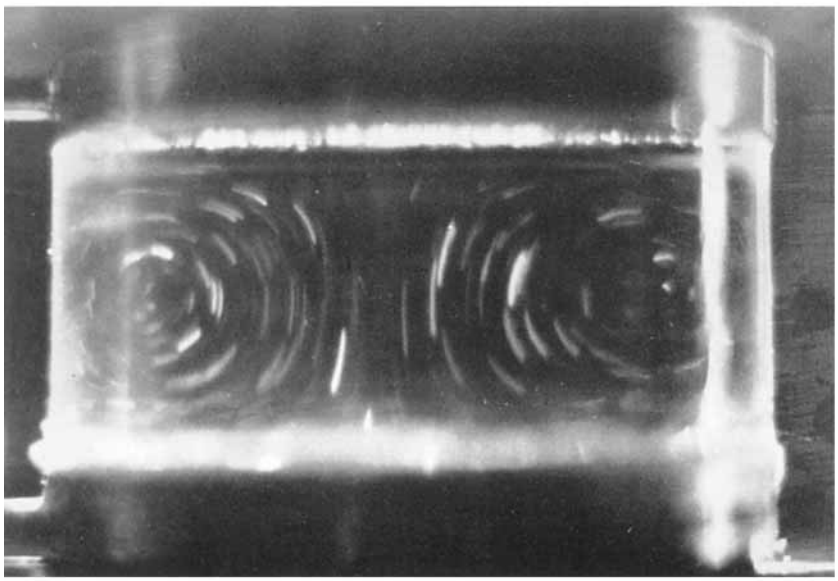

(*b*)

FIGURE 3. Solid-isothermal upper surface. (*a*) Downflow at the centre, $R = 8000$. (*b*) Upflow at the centre, $R = 8200$.